



Published in final edited form as:

*Bioorg Med Chem Lett.* 2018 April 01; 28(6): 1024–1029. doi:10.1016/j.bmcl.2018.02.027.

## Structure-based design and biological evaluation of inhibitors of the *Pseudomonas aeruginosa* heme oxygenase (*pa*-HemO)

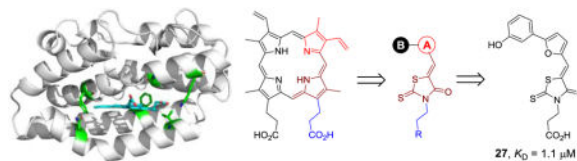
Dongdong Liang<sup>a,§</sup>, Elizabeth Robinson<sup>a,§</sup>, Kellie Hom<sup>a</sup>, Wenbo Yu<sup>a</sup>, Nam Nguyen<sup>a</sup>, Yue Li<sup>b</sup>, Qianshou Zong<sup>c</sup>, Angela Wilks<sup>a,\*</sup>, and Fengtian Xue<sup>a,\*</sup>

<sup>a</sup>Department of Pharmaceutical Sciences, University of Maryland School of Pharmacy, Baltimore, Maryland 21201, United States

<sup>b</sup>Department of Chemistry and Biochemistry, University of Maryland College Park, College Park 20740, United States

<sup>c</sup>College of Biological and Chemical Sciences and Engineering, Jiaying University, Jiaying City, Zhejiang 314001, People's Republic of China

### Graphical abstract



*Pseudomonas aeruginosa* is an opportunistic Gram-negative bacterial and one of the most common causes of hospital-acquired infections worldwide.<sup>1,2</sup> It is the major human pathogen that leads to severe lung deterioration in cystic fibrosis (CF) patients.<sup>3</sup> The treatment of *Pseudomonas* is further complicated by its resistance to most available antibiotics.<sup>4</sup> For *P. aeruginosa* infections polymyxins B and E (colistin) are the only choices of antibiotics despite their high toxicity.<sup>5</sup> Therefore, it is urgent to develop new therapeutic agents for MDR *P. aeruginosa*.

Iron is an essential nutrient for survival and virulence of *P. aeruginosa*.<sup>6</sup> It regulates a number of virulence factors in *P. aeruginosa* including exotoxins, proteases, and biofilm formation.<sup>7–10</sup> Within the host iron is not readily available due to sequestration by iron binding proteins such as transferrin and ferritin or in the form of heme.<sup>11</sup> However *Pseudomonas* overcomes this situation through a variety of mechanisms including the secretion of siderophores (pyoverdine and pyochelin),<sup>12,13</sup> ferrous iron uptake (Feo),<sup>14</sup> and its unique heme acquisition systems.<sup>15–19</sup>

\*Corresponding authors: A. Wilks, awilks@rx.umaryland.edu; F.Xue, fxue@rx.umaryland.edu.

§D.L. and E.R. contributed equally to this work.

**Publisher's Disclaimer:** This is a PDF file of an unedited manuscript that has been accepted for publication. As a service to our customers we are providing this early version of the manuscript. The manuscript will undergo copyediting, typesetting, and review of the resulting proof before it is published in its final citable form. Please note that during the production process errors may be discovered which could affect the content, and all legal disclaimers that apply to the journal pertain.

As part of the heme acquisition system, heme degradation by the enzyme heme oxygenase (HemO) is essential for *P. aeruginosa* to acquire iron from the host.<sup>20</sup> *P. aeruginosa* HemO (*pa*-HemO) catalyzes the reaction to breakdown heme and release iron, along with CO and  $\beta$ - and  $\delta$ -biliverdin.<sup>20</sup> It has also been shown by the Wilks Lab that the catalytic activity of *pa*-HemO was pivotal to drive the metabolic flux of heme into the cell.<sup>21–23</sup> Furthermore, the *P. aeruginosa hemO* isogenic mutant, or a strain complemented with a non-functional *pa*-HemO, showed significant attenuation of infection in a mouse lung infection model, when compared to the wild type strain (unpublished results). This data suggests *pa*-HemO inhibitors, by blocking a key mechanism of the iron acquisition system, represents a promising therapeutic target for *P. aeruginosa* infections.

Small molecule inhibitors of *pa*-HemO have been reported.<sup>24–26</sup> These inhibitors achieved activities by binding either to the heme-binding active site<sup>25</sup> or an allosteric site<sup>26</sup> depending on their structural features. Most of these known inhibitors are close derivatives of high throughput screen (HTS) hits, which commonly suffer from major drawbacks such as modest potency ( $K_D$  20–50  $\mu\text{M}$ ) and poor pharmacological properties. For instance, we recently reported *pa*-HemO inhibitor **1** (Fig. 1), with the  $K_D$  value of 18.4  $\mu\text{M}$  and limited chemical stability.<sup>25</sup>

The *pa*-HemO has a unique heme-binding active site. The solvent accessible surface of *pa*-HemO ( $\sim 7.5 \text{ \AA}^3$ ) is much smaller than the mammalian enzyme HO1 (43.6–59.7  $\text{ \AA}^3$ ).<sup>27–30</sup> More interestingly, different to the binding mode in human HO1 (Fig. 2A) and other known isozymes, heme binds in the *pa*-HemO active site with a dramatically rotated ( $\sim 100$  degrees) orientation<sup>28</sup> as a result of the unique amino acid network present in the active site (Fig. 2B). These structural differences provide opportunities for selective inhibition of the *pa*-HemO over other HemOs such as HO1.<sup>31</sup>

To take advantage of the unique active site of *pa*-HemO, we designed a series of inhibitors (**2–31**) based on a 3-(4-oxo-2-thioxothiazolidin-3-yl)propanoic acid scaffold (Fig. 3). New compound design was directed by the computer-aided drug design (CADD) Site Identification by Ligand Competitive Saturation (SILCS) method as reported previously.<sup>26</sup> The carboxylic acid or tetrazole groups of compounds **2–31** mimic one of the two acid groups of heme, to form an electrostatic interaction with the basic residue Lys<sup>132</sup> of *pa*-HemO. The 4-oxo-2-thioxothiazolidin-3-yl fragment (shown in brown) is chosen to mimic one of the pyrrole rings of the porphyrin, to fit into the hydrophobic binding pocket around Val<sup>33</sup> (Fig. 2B). The same moiety could also form potential interaction with the iron-chelating residue His<sup>26</sup> of *pa*-HemO. We note the controversial reports on the application of rhodanine in medicinal chemistry;<sup>32,33</sup> studies in our lab to modify the rhodanine are ongoing. The substituted A-ring is selected to interact with the hydrophobic pocket next to residues Phe<sup>189</sup> and Q<sup>52</sup>, while the extended tail B-ring is employed to extend the compound to interact with residues Phe<sup>117</sup> and Asn<sup>19</sup> of *pa*-HemO.

To test our hypothesis, we first synthesized two pyridinyl compounds **2** and **3** (Fig. 4A). Compounds **2** and **3** indicated modest affinities to *pa*-HemO with the  $K_D$  values of 51  $\mu\text{M}$  and 27  $\mu\text{M}$ , respectively, using the previously established fluorescence quenching assay.<sup>26</sup> The potency of the tetrazole analog **3** was almost 2-fold higher than that of the carboxylic

inhibitor **2**. We reasoned that the enhancement in potency might be due to the presence of residue Phe<sup>128</sup> next to Lys<sup>132</sup> (Fig. 2B), which can form additional  $\pi$ - $\pi$  stacking interaction with the tetrazole fragment of inhibitor **3**. We then performed saturation transfer difference-nuclear magnetic resonance (STD-NMR) experiments to confirm the binding of compound **3** to *pa*-HemO, and found that both the pyridine moiety and aliphatic tail of the inhibitor show clear binding to the enzyme (Fig. 4B). To further characterize the interaction between inhibitor **3** and *pa*-HemO, we carried out <sup>1</sup>H,<sup>15</sup>N-HSQC NMR experiments (Fig. 4C). The presence of compound **3** caused multiple chemical shift perturbations (CSPs) in the heme binding site of *pa*-HemO. Interestingly residues with CSP over 3 fold of standard deviation ( $\sigma$ ), including Leu<sup>32</sup>, Ser<sup>35</sup>, Lys<sup>36</sup>, Phe<sup>39</sup>, Arg<sup>85</sup>, Glu<sup>104</sup>, Ser<sup>119</sup>, Glu<sup>137</sup>, Asn<sup>141</sup>, Phe<sup>189</sup>, Gly<sup>190</sup> and Arg<sup>195</sup>, are mostly located in the vicinity of the heme-binding active site (Fig. 4C). Of them only Arg<sup>85</sup> and Glu<sup>104</sup> locate on the back surface of the enzyme. The strong CSPs of these two residues can be results of the configuration change of the enzyme upon inhibitor binding. Overall, the results show that compound **3** binds to the active site with modest affinity, suggesting that the scaffold can be suitable developing inhibitors for *pa*-HemO.

As shown in Scheme 1, Knoevenagel condensation of selected aromatic aldehydes (**32**) with 3-(4-oxo-2-thioxothiazolidin-3-yl)ethylene derivatives (**33a-d**) in the presence of 10 equivalents of sodium acetate (NaOAc) in acetic acid (AcOH) gave compounds **2-23** and **28-31** in good to excellent yields upon heating. The synthesis of compounds **24-27** has been achieved using a two-step procedure. Suzuki coupling of boronic acid **34** with substituted iodobenzenes in the presence of Pd(0) catalyst generated compound **35** in modest to good yields. Aldehyde **35** was then submitted to Knoevenagel condensation to provide inhibitors **24-27** in good yields.

Compared to inhibitor **2**, the 2-furan analog **4** was slightly more potent, while the catechol analog **5** indicated similar activity (Table 1). Similar to the results of the tetrazole inhibitor **3**, slightly enhanced affinities were observed when the carboxylic acid groups of compounds **4** and **5** were replaced by the aromatic acid bioisostere tetrazole. Introduction of an electrodonating methoxy substitution at either the *m*- (**8**) or *p*-position (**9**) generated new inhibitors with ~2-fold improved inhibitory potency. The *p*-F substituted analog **10** indicated similar affinity to that of inhibitor **2**. Larger halogen Cl-substitution at the same position yielded compound **11** with > 3-fold increased affinity, although the diCl-substituted analog **12** didn't further improve the potency. The aliphatic *p*-Pr analog **13** showed a 5-fold improvement in potency compared to compound **2**. Despite of the decreased potency of the 1-naphthyl analog **14**, the 2-naphthyl analog **15** showed a  $K_D$  value of 3.9  $\mu$ M. Similarly good potency was observed with the indole analog **16**.

To explore inhibitors with potential interactions to the hydrophobic pocket formed by Phe<sup>117</sup> and Asn<sup>19</sup>, a collection of 11 new inhibitors (**17-27**) were synthesized with a B-ring included in their chemical structures (Table 2). We first tested structurally rigid bi-Ph compounds **17** and **18**. The *m*-Ph analog **17** indicated a significant decrease of the inhibitory potency, however, the *p*-Ph compound **18** indicated a promising  $K_D$  value of 3.3  $\mu$ M. With the introduction of a flexible linker between the A- and B-rings, compounds **19-22** were

synthesized and tested. The results indicated that the *m*-PhNH analog **21** gave the best inhibitory potency with a  $K_D$  value of 1.2  $\mu\text{M}$ . We have also studied inhibitors with extended chemical structures based upon the furan analog **4** (**23–27**). While the *p*-methylester-Ph substitution (**23**) significantly diminished the inhibitory potency, the same substituent at the *m*-position led to compound **25** with a  $K_D$  value of 7.6  $\mu\text{M}$ . The CN group (**26**) at the same position was detrimental to the binding affinity. The *m*-OH substituted analog gave the most potent compound **27** with a  $K_D$  value of 1.1  $\mu\text{M}$ , which is similar to the value of the substrate heme.<sup>24</sup>

Given the availability of the assay results, further analysis of the utility of the SILCS LGFE scores was undertaken (Fig. 5). Correlation analysis and calculation of the predictive index (PI)<sup>34</sup> with respect to LGFE scores were performed. Based on all compounds in Tables 1–2, this analysis results in a high PI  $\sim$  0.70 and  $R^2 \sim$  0.53 for the correlation between LGFE and  $K_D$  as shown in Fig. 5. This indicates FragMaps are of utility with respect to both qualitatively directing ligand design and yield a reasonable level of quantitative predictability, indicating the utility of the approach in the further refinement of the presented compounds.

The binding sites of inhibitors **18**, **21**, and **27** were studied using both SILCS calculation (Fig. S1) and  $^1\text{N}$ ,  $^{15}\text{N}$ -HSQC NMR experiments (Fig. 6 and Tables S2–S5). With the presence of inhibitor **18**, significant CSPs ( $> 3\sigma$ ) were observed for residues N19, L32, S35, K36, Q52, E104, V118, S119, S183, A185, and R195 (Fig. 6A and S2). All these residues are located in the vicinity to the heme binding active site of *pa*-HemO. Perturbation of six residues, L32, S35, K36, E104, S119 and R195 were also detected for inhibitor **3**, suggesting that these inhibitors may bind to the same binding site of the enzyme. Compared to inhibitor **18**, the addition of inhibitor **21** led to significant CSPs for less residues including L32, Q52, E104, L116, S119, L177, S183, L193 and R195 (Fig. 6B and S3). Most of these residues overlap with those for compounds **3** and **18**, indicating that compound **21** likely adapts similar binding mode in the heme binding site of the *pa*-HemO. The presence of inhibitor **27** caused significant CSP for *pa*-HemO residues L18, E37, A40, Q56, L68, S77, L113, G190, and F197 (Fig. 6C and S4). In addition,  $^1\text{N}$ ,  $^{15}\text{N}$ -HSQC peaks of heme binding site residues L32, Q52, S119 and R195 disappeared due to their fast exchange rate. These results indicated that upon the binding of inhibitor **27**, the heme binding site of *pa*-HemO becomes more flexible.

The anti-pseudomonas activity of the three most potent compounds, **21**, **27**, and **18** were evaluated using both the MIC<sub>50</sub> by growing *P. aeruginosa* in minimal media supplemented with heme or free iron, and biofilm formation assays (Table 3). Our results indicated all three compounds showed poor anti-bacterial effects on pseudomonas in both assays. We reasoned that the presence of the carboxylic acid group in these compounds might prohibit the in vivo effects of inhibitors, as evidenced in a number of previous studies.<sup>34,35</sup> It has been well documented that compounds, with in vivo activities toward pseudomonas, usually employs basic amino groups.<sup>35</sup> Therefore, we have synthesized and tested compounds **30** and **31**, which showed  $K_D$  values of 43 and 18  $\mu\text{M}$ , respectively. However, these compounds also did not have significant antibacterial activity.

In summary, 4-Oxo-2-thioxothiazolidin-3-yl-propanoic acid based inhibitors of *pa*-HemO are described to interact with the unique network of residues in the heme-binding active site of the enzyme. SAR efforts of the series resulted in analogs **21** and **27**, with around 1  $\mu$ M affinities. NMR studies confirmed the binding site of selected inhibitors of the family, which is consistent with the results obtained from computational analyses. Further structure optimization is undergoing for anti-microbial activities of inhibitors.

## Supplementary Material

Refer to Web version on PubMed Central for supplementary material.

## Acknowledgments

We thank the National Health Institute grant #AI102883 to A.W., and Dr. Amanda Oglesby-Sherrouse for advice on the biofilm formation assays.

## References and Notes

1. Kerr KG, Snelling AM. *J Hosp Infect.* 2009; 73:338–344. [PubMed: 19699552]
2. Salter SJ. *Nat Rev Microbiol.* 2015; 13:69. [PubMed: 25549963]
3. Costerton JW. *Trends Microbiol.* 2001; 9:50–52. [PubMed: 11173226]
4. Obritsch MD, Fish DN, MacLaren R, Jung R. *Antimicrob Agents Chemother.* 2004; 48:4606–4610. [PubMed: 15561832]
5. Falagas ME, Kasiakou SK. *Clin Infect Dis.* 2005; 40:1333–1341. [PubMed: 15825037]
6. Minandri F, Imperi F, Frangipani E, Bonchi C, Visaggio D, Facchini M, Pasquali P, Bragonzi A, Visca P. *Infect Immun.* 2016; 84:2324–2335. [PubMed: 27271740]
7. Cox CD. *Infect Immun.* 1982; 36:17–23. [PubMed: 6804387]
8. Meyer JM, Neely A, Stintzi A, Georges C, Holder IA. *Infect Immun.* 1996; 64:518–523. [PubMed: 8550201]
9. Takase H, Nitanai H, Hoshino K, Otani T. *Infect Immun.* 2000; 68:4498–4504. [PubMed: 10899848]
10. Takase H, Nitanai H, Hoshino K, Otani T. *Infect Immun.* 2000; 68:1834–1839. [PubMed: 10722571]
11. Otto BR, Verweij-van Vught AM, MacLaren DM. *Crit Rev Microbiol.* 1992; 18:217–233. [PubMed: 1532495]
12. Heinrichs DE, Young L, Poole K. *Infect Immun.* 1991; 59:3680–3684. [PubMed: 1910015]
13. Royt PW. *Biol Met.* 1990; 3:28–33. [PubMed: 2119198]
14. Marlovits TC, Haase W, Herrmann C, Aller SG, Unger VM. *Proc Natl Acad Sci U S A.* 2002; 99:16243–16248. [PubMed: 12446835]
15. Ochsner UA, Johnson Z, Vasil ML. *Microbiology.* 2000; 146:185–198. [PubMed: 10658665]
16. Bhakta MN, Wilks A. *Biochemistry-U.S.* 2006; 45:11642–11649.
17. Block DR, Lukat-Rodgers GS, Rodgers KR, Wilks A, Bhakta MN, Lansky IB. *Biochemistry-U.S.* 2007; 46:14391–14402.
18. Lansky IB, Lukat-Rodgers GS, Block D, Rodgers KR, Ratliff M, Wilks A. *J Biol Chem.* 2006; 281:13652–13662. [PubMed: 16533806]
19. O'Neill MJ, Bhakta MN, Fleming KG, Wilks A. *Proc Natl Acad Sci U S A.* 2012; 109:5639–5644. [PubMed: 22451925]
20. Choby JE, Skaar EP. *J mol biol.* 2016; 428:3408–3428. [PubMed: 27019298]
21. Barker KD, Barkovits K, Wilks A. *J Biol Chem.* 2012; 287:18342–18350. [PubMed: 22493498]
22. Kaur AP, Lansky IB, Wilks A. *J Biol Chem.* 2009; 284:56–66. [PubMed: 18990702]
23. O'Neill MJ, Wilks A. *ACS Chem Biol.* 2013; 8:1794–1802. [PubMed: 23947366]

24. Furci LM, Lopes P, Eakanunkul S, Zhong SJ, MacKerell AD, Wilks A. *J Med Chem.* 2007; 50:3804–3813. [PubMed: 17629261]
25. Hom K, Heinzl GA, Eakanunkul S, Lopes PEM, Xue F, MacKerell AD, Wilks A. *J Med Chem.* 2013; 56:2097–2109. [PubMed: 23379514]
26. Heinzl GA, Huang W, Yu W, Giardina BJ, Zhou Y, MacKerell AD, Wilks A, Xue F. *J Med Chem.* 2016; 59:6929–6942. [PubMed: 27353344]
27. Friedman J, Lad L, Deshmukh R, Li H, Wilks A, Poulos TL. *J Biol Chem.* 2003; 278:34654–34659. [PubMed: 12819228]
28. Friedman J, Lad L, Li H, Wilks A, Poulos TL. *Biochemistry-US.* 2004; 43:5239–5245.
29. Schuller DJ, Wilks A, de Montellano PRO, Poulos TL. *Nat Struct Biol.* 1999; 6:860–867. [PubMed: 10467099]
30. Schuller DJ, Zhu W, Stojiljkovic I, Wilks A, Poulos TL. *Biochemistry-US.* 2001; 40:11552–11558.
31. Ratliff M, Zhu W, Deshmukh R, Wilks A, Stojiljkovic I. *J Bacteriol.* 2001; 183:6394–6403. [PubMed: 11591684]
32. Baell JB, Holloway GA. *J Med Chem.* 2010; 53:2719–2740. [PubMed: 20131845]
33. Mendgen T, Steuer C, Klein CD. *J Med Chem.* 2012; 55:743–753. [PubMed: 22077389]
34. Wagner S, Sommer R, Hinsberger S, Lu C, Hartmann RW, Empting M, Titz A. *J Med Chem.* 2016; 59:5929–5969. [PubMed: 26804741]
35. Richter MF, Drown BS, Riley AP, Garcia A, Shirai T, Svec RL, Hergenrother PJ. *Nature.* 2017; 545:299–304. [PubMed: 28489819]

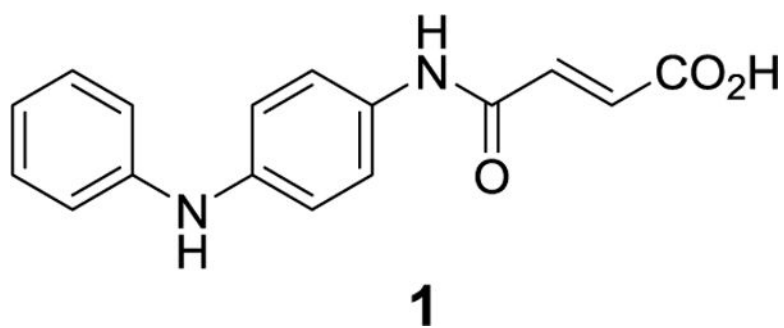


**Fig. 1.**  
Chemical structure of the *pa*-HemO inhibitor **1**.

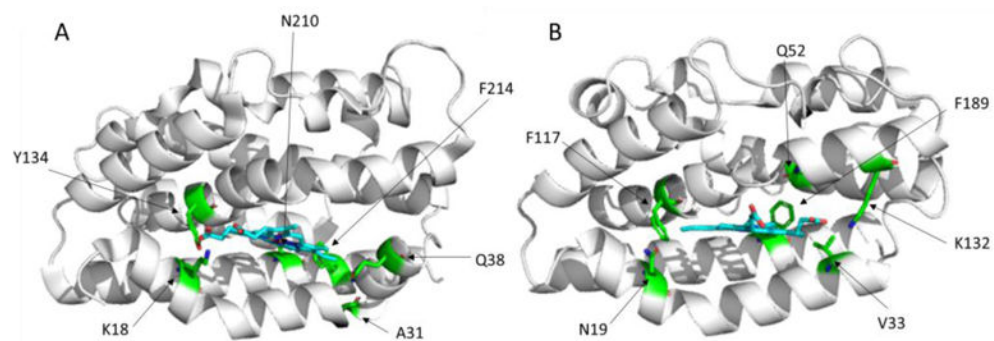


**Fig. 2.**  
Heme-binding active sites of A) HO1 (PDB 1N45) and B) *pa*-HemO (PDB 1SK7).



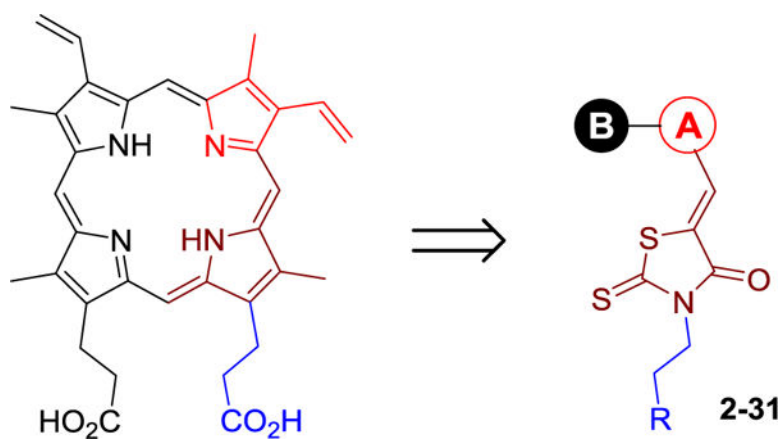


**Fig. 3.**  
Design and general structure of new inhibitors 2-31.

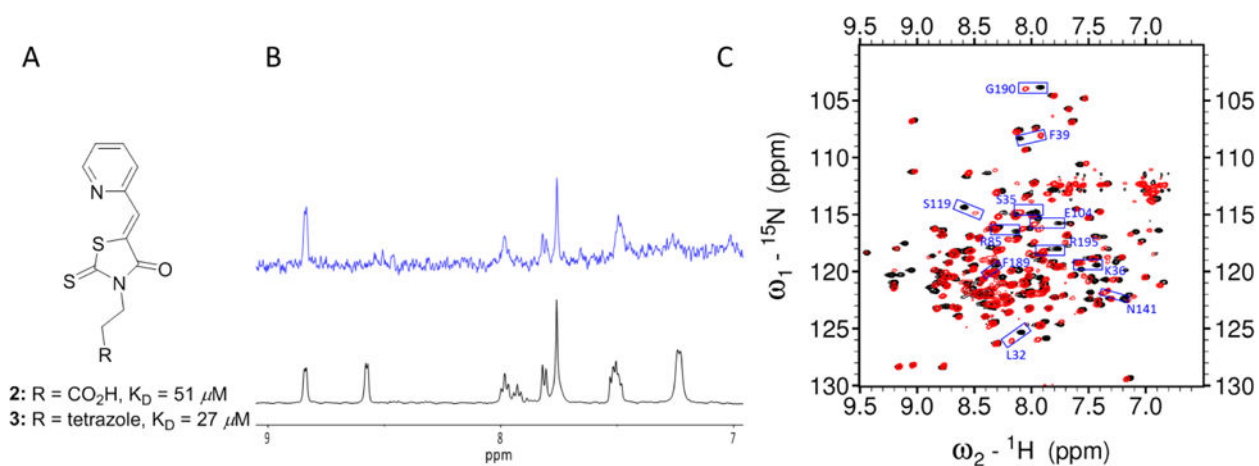


**Fig. 4.** Characterization of initial compounds 2–3. A) Chemical structures and  $K_D$  values of compounds 2–3 in the fluorescence quenching assays. B) STD-NMR experiment results: <sup>1</sup>H spectra (black) and the STD spectrum (blue) of compound 3. Note that the <sup>1</sup>H NMR of compound 3 indicated a mixture of two rotamers with estimation of 1:1 ratio. One of the two rotamers binds favorably to apo *pa*-HemO. C) <sup>1</sup>H, <sup>15</sup>N-HSQC NMR results of compound 3. Black: apo *pa*-HemO; Red: compound 3 mixed with apo *pa*-HemO.

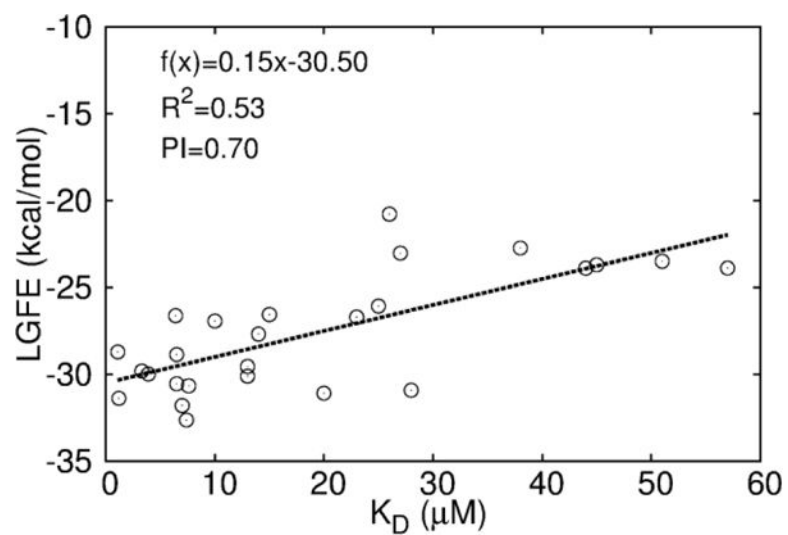


**Fig. 5.** Correlation plots between  $\text{LGFE}$  and  $K_D$ . Coefficient of determination ( $R^2$ ) and predictive index (PI) are shown for the quality of correlation.

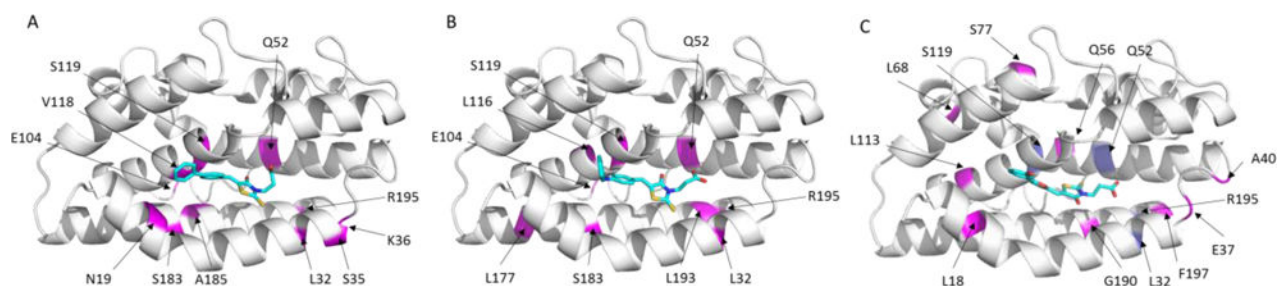
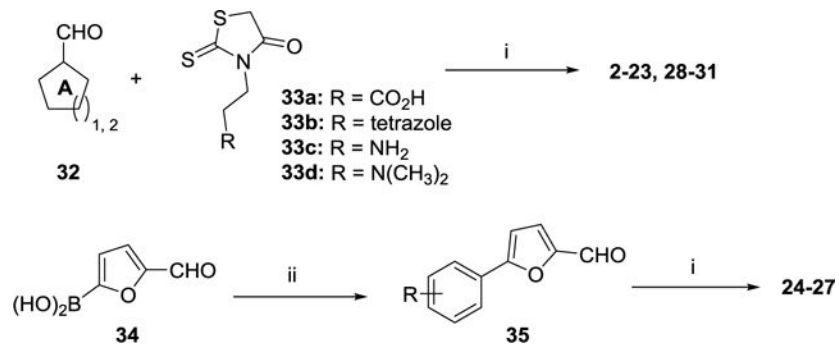


**Fig. 6.**

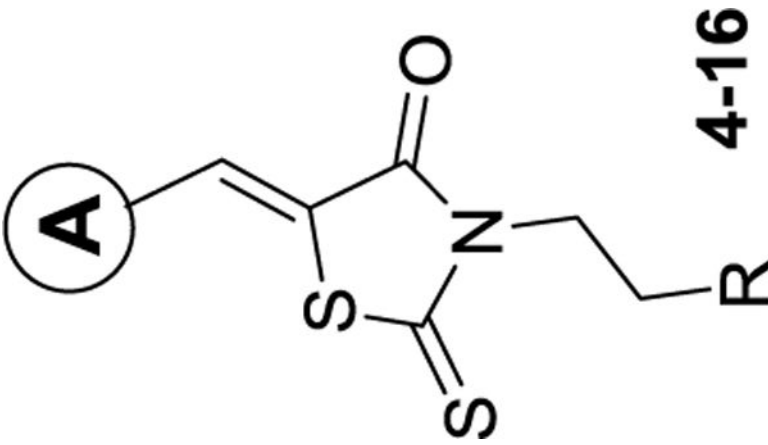
A representation of the *pa*-HemO based on Protein Data Bank structure (PDB: 1SK7) is shown, indicating residues perturbed upon binding of compounds **18** (A), **21** (B), and **27** (C). (A) In magenta, residues with  $>3\sigma$  chemical shift perturbations listed as the following in increasing order: A84, Q52, L116, L193, L177, E104, S183, R195, L32, and S119. (B) In magenta, residues with  $>3\sigma$  chemical shift perturbations listed as the following in increasing order: K36, Q52, A185, V118, R195, L32, S35, S119, N19, S119 and E104. (C) In magenta, residues with  $>3\sigma$  chemical shift perturbations listed as the following in increasing order: A185, E37, S77, G190, Q56, L113, L68, A40, L18 and F197. In blue, residues L32, Q52, S119 and R195 (shown in purple) disappeared due to the fast exchange rate.



**Scheme 1.**

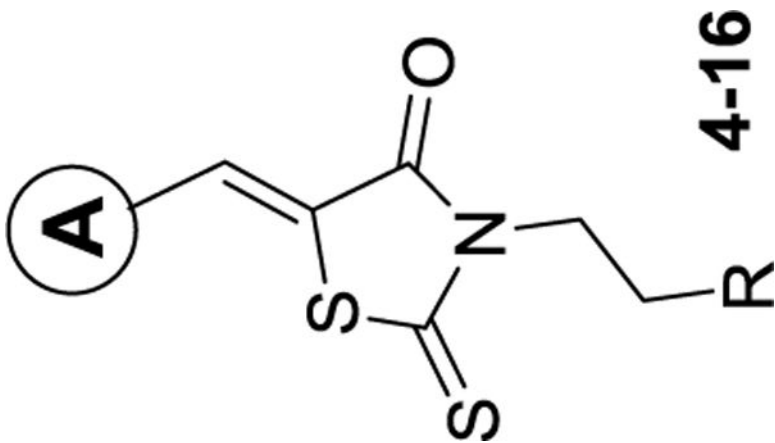
Synthesis of compounds **2–31**. Reagents and conditions: (i) 3-(4-oxo-2-thioxothiazolidin-3-yl)propanoic acid, NaOAc:AcOH (1:10), 105 °C, 6–14 h, 47–87%; (ii) iodobenzene, Pd(PPh<sub>3</sub>)<sub>2</sub>Cl<sub>2</sub>, K<sub>2</sub>CO<sub>3</sub>, dioxane:H<sub>2</sub>O (3:1), 100 °C, overnight, 71–87%.

Table 1

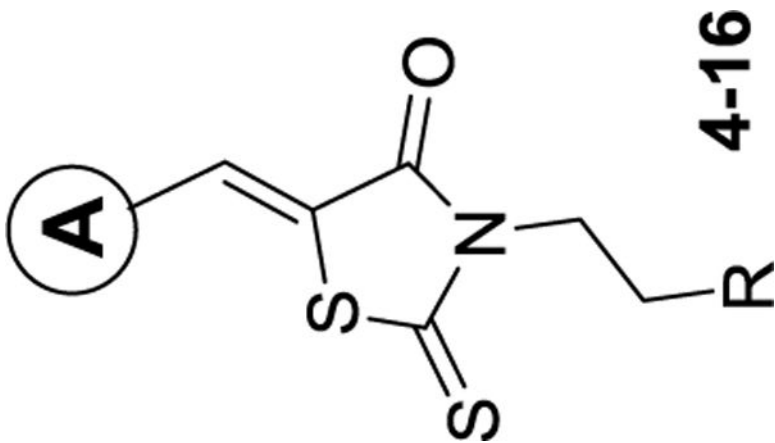
Structure features, calculated properties,  $K_D$  values of compounds 4-16



compd	A	R	LGFE <sup>a</sup> (kcal/mol)	LE <sup>a</sup>	$K_D^b$ ( $\mu$ M)
4		-CO <sub>2</sub> H	-22.7	-1.26	38 ± 10
5		tetrazole	-20.8	-1.04	26 ± 6
6		-CO <sub>2</sub> H	-23.9	-1.14	57 ± 8
7		tetrazole	-23.7	-1.03	45 ± 6

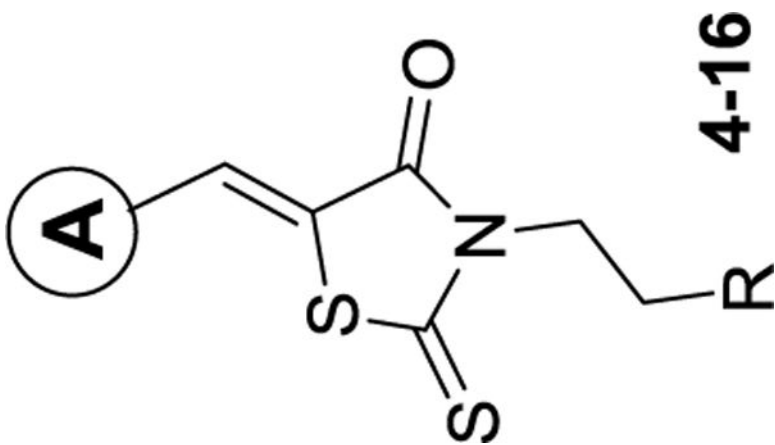


compd	A	R	LGFE <sup>a</sup> (kcal/mol)	LF <sup>a</sup>	K <sub>D</sub> <sup>b</sup> (μM)
8		-CO <sub>2</sub> H	-26.1	-1.24	25 ± 8
9		-CO <sub>2</sub> H	-26.7	-1.27	23 ± 4
10		-CO <sub>2</sub> H	-23.9	-1.19	44 ± 9



compd	A	R	LGFE <sup>a</sup> (kcal/mol)	LF <sup>a</sup>	K <sub>D</sub> <sup>b</sup> (μM)
11		-CO <sub>2</sub> H	-26.6	-1.33	15 ± 2
12		-CO <sub>2</sub> H	-27.7	-1.32	14 ± 4
13		-CO <sub>2</sub> H	-26.9	-1.22	10 ± 4





cmpd	A	R	LGFE <sup>a</sup> (kcal/mol)	LE <sup>a</sup>	K <sub>D</sub> <sup>b</sup> (μM)
14		-CO <sub>2</sub> H	-29.6	-1.28	13 ± 2
15		-CO <sub>2</sub> H	-30.0	-1.30	3.9 ± 1
16		-CO <sub>2</sub> H	-26.6	-1.21	6.4 ± 1.4

<sup>a</sup> Ligand Grid Free Energy (LGFE) and Ligand Efficiency (LE) calculated with SILCS.<sup>26</sup>

The listed result was the average of three independent experiments.  
*q*

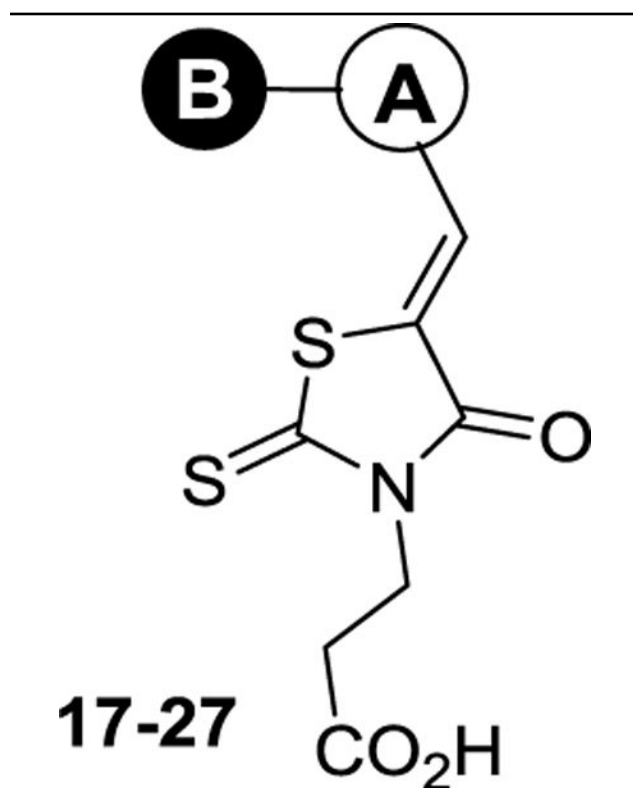
Author Manuscript

Author Manuscript

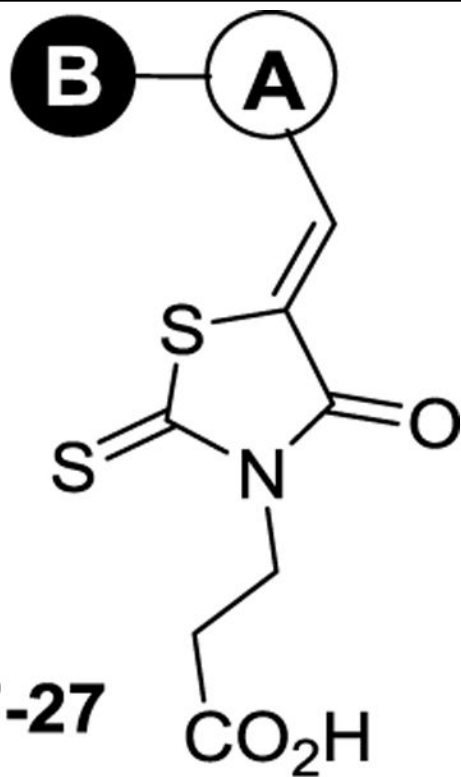
Author Manuscript

Author Manuscript

Table 2

Structure features, calculated properties,  $K_D$  values of compounds 17–27

compd	A-B	LGFE <sup>a</sup> (kcal/mol)	LE <sup>a</sup>	K <sub>D</sub> <sup>b</sup> (μM)
17		-31.1	-1.24	20±2
18		-29.8	-1.19	3.3 ± 0.9
19		-31.8	-1.22	7.0 ± 2.7
20		-30.5	-1.17	6.5 ± 1.3
21		-31.4	-1.21	1.2 ± 0.2
22		-32.6	-1.13	7.4 ± 0.6



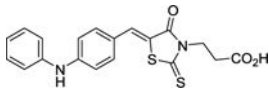
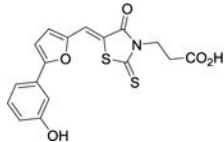
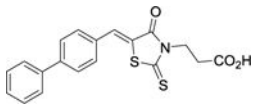
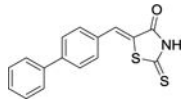
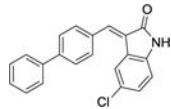
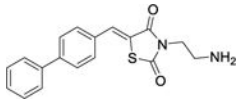
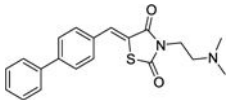
compd	A-B	LGFE <sup>a</sup> (kcal/mol)	LE <sup>a</sup>	K <sub>D</sub> <sup>b</sup> (μM)
23		-30.9	-1.10	28 ± 6
24		-28.9	-1.00	6.5 ± 1.0
25		-30.7	-1.10	7.6 ± 1.1
26		-30.1	-1.16	13 ± 1.4
27		-28.7	-1.15	1.1 ± 0.2

<sup>a</sup>Ligand Grid Free Energy (LGFE) and Ligand Efficiency (LE) calculated with SILCS.<sup>26</sup>

<sup>b</sup>The listed result was the average of three independent experiments.

Table 3

Structure features and properties of compounds 28–31

compd	structure	$K_D^a$ ( $\mu\text{M}$ )	$\text{MIC}_{50}$ ( $\mu\text{g/mL}$ )	Biofilm assay ( $\mu\text{g/mL}$ )
21		$1.2 \pm 0.2$	> 300	> 300
27		$1.1 \pm 0.2$	> 300	> 300
18		$3.3 \pm 0.9$	> 300	> 300
28		$2.3 \pm 0.5$	NA <sup>b</sup>	> 300
29		$5.2 \pm 0.7$	NA <sup>b</sup>	> 300
30		$43 \pm 11$	> 300	> 300
31		$18 \pm 3$	NA <sup>b</sup>	> 300

<sup>a</sup>The listed result was the average of three independent experiments.

<sup>b</sup>NA refers to no microbial inhibition activity occurred.